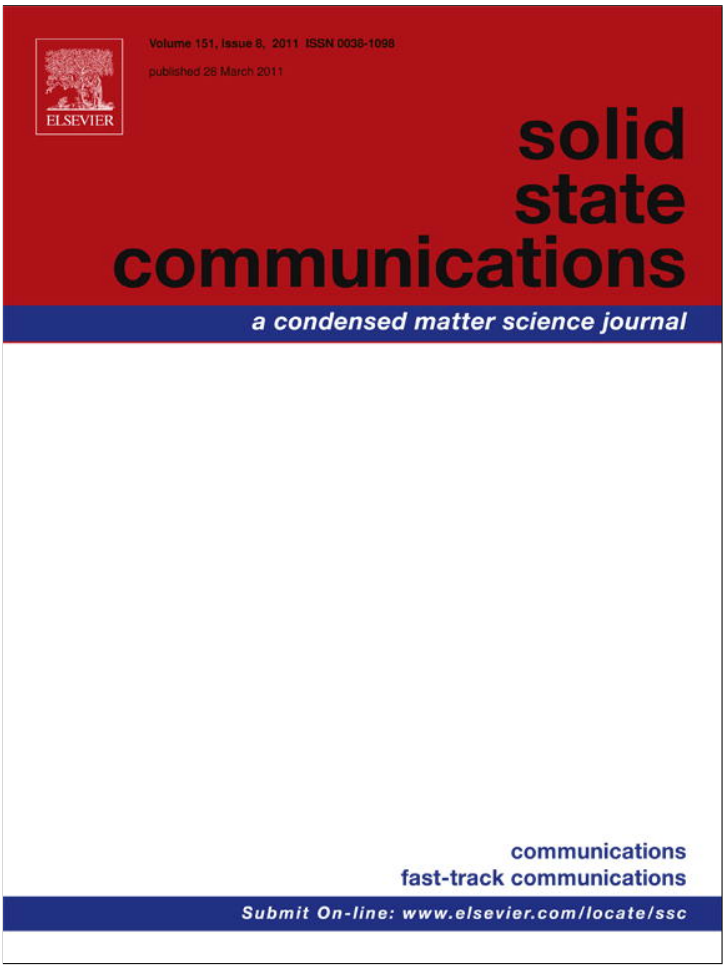

Solid State Communications 151 (2011) 624–627

Contents lists available at ScienceDirect

Solid State Communications

journal homepage: www.elsevier.com/locate/ssc

Enhanced room temperature ferromagnetism in porous $BiFeO_3$ prepared using cotton templates

Qingyu Xu [a,*], Xiaohong Zheng [a], Zheng Wen [b], Yi Yang [c], Di Wu [b], Mingxiang Xu [a]

[a] Department of Physics, Southeast University, Nanjing 211189, China
[b] Department of Materials Science and Engineering, Nanjing University, Nanjing 210008, China
[c] Department of Physics, Nanjing University, Nanjing 210008, China

ARTICLE INFO

Article history:
Received 18 December 2010
Received in revised form
21 December 2010
Accepted 28 January 2011
by A. Pinczuk
Available online 16 February 2011

Keywords:
A. Ferroelectrics
A. Magnetic ordered materials
B. Chemical synthesis
D. Exchange and superexchange

ABSTRACT

Porous $BiFeO_3$ has been prepared using cotton templates. Strongly enhanced ferromagnetism with saturate magnetization of 3 emu/g at 300 K has been observed. An energy band gap of 2.21 eV was determined from the UV–visible diffuse reflectance spectrum. The Raman and X-ray photoelectron spectroscopy measurements indicate the existence of Fe^{2+} and the suppression of the oxygen octahedral tilts. The enhanced ferromagnetism has been attributed to the enhanced double exchange interaction with increased angle of Fe^{2+}–O–Fe^{3+}.

1. Introduction

$BiFeO_3$ is one of the most widely studied multiferroic materials with ferroelectric Curie temperature of $T_c \sim 1103$ K and antiferromagnetic Neel temperature $T_N \sim 643$ K [1,2]. $BiFeO_3$ has a *G*-type antiferromagnetic spin structure with a superimposed cycloidal modulation with a period of about 62 nm, the macroscopic magnetization has been averaged to zero, though there is a small canting between the antiferromagnetic arrangement of the neighboring spins of Fe^{3+} [3]. Thus the magnetization is very weak, which inhibits the observation of linear magnetoelectric effect [4]. Much work has been done to enhance the ferromagnetism which has been considered to be important to utilize the room temperature multiferroicity of $BiFeO_3$ [5]. For example, enhanced room temperature ferromagnetism has been observed in nanostructure $BiFeO_3$ with size below 62 nm [5,6], or Bi site substitution with bigger ions to induce structural distortion [7,8], to suppress the cycloidal structure. In this paper, we present a new method to prepare the porous $BiFeO_3$ using cotton templates. Strongly enhanced room temperature ferromagnetism has been observed which was attributed to the enhanced double exchange Fe^{2+}–O–Fe^{3+} interaction.

2. Experiment

Porous $BiFeO_3$ was prepared by a tartaric acid modified sol–gel technique [9], with cotton as templates. Equimolar amounts of $Bi(NO_3)_3 \cdot 5H_2O$ and $Fe(NO_3)_3 \cdot 9H_2O$ were dissolved in diluted HNO_3 solution. Tartaric acid in 1:1 molar ratio with respect to metal nitrates was added to the solution. The cotton templates were immersed in the solution under ultrasonic vibration for 5 h. The filled templates were washed in the deionized water, then dried at 160 °C for 2 h, and heat treated in air at 600 °C for 2 h. The products were leached in diluted HNO_3 solution to remove the impurity of $Bi_{25}FeO_{39}$ [10], and then washed in deionized water and ethanol repeatedly. The final products (BFO-600) were dried at 160 °C and used for the magnetic and structural characterizations. For comparison, $BiFeO_3$ powders without using cotton templates (BFO-500) were also prepared with sintering temperature of 500 °C for 2 h. The structures of samples were studied by X-ray diffraction (XRD) with Cu Kα radiation and scanning electron microscope (SEM). Raman measurements were carried out on a Horiba Jobin Yvon LabRAM HR 800 micro-Raman spectrometer. The valence states of the constituent ions were studied by X-ray photoelectron spectroscopy (XPS, ThermoFisher SCIENTIFIC). The magnetization was measured by a physical property measurement system (PPMS-9, Quantum Design).

* Corresponding author. Tel.: +86 2552090600; fax: +86 2552090600.
E-mail address: xuqingyu@seu.edu.cn (Q. Xu).

0038-1098/$ – see front matter © 2011 Elsevier Ltd. All rights reserved.
doi:10.1016/j.ssc.2011.01.029

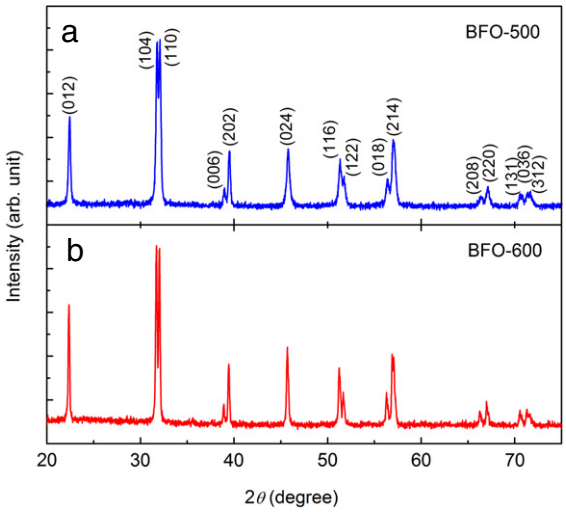

Fig. 1. XRD patterns of (a) BFO-500 and (b) BFO-600.

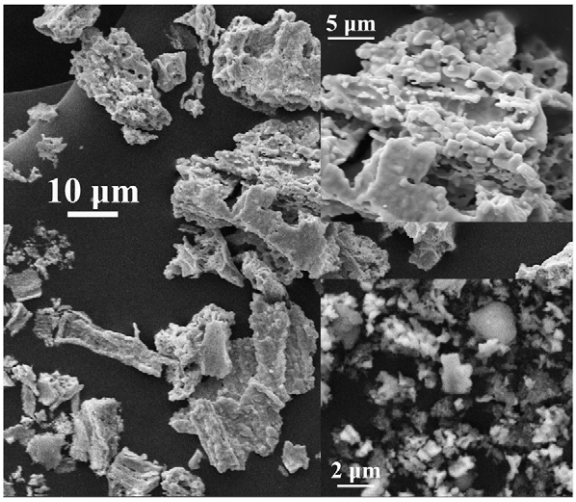

Fig. 2. SEM image of $BiFeO_3$ prepared using cotton template before leaching in diluted HNO_3, top inset shows the enlarged view, the bottom inset shows the SEM image of BFO-600 ($BiFeO_3$ prepared using cotton template after leaching in diluted HNO_3).

3. Results and discussion

Fig. 1 shows the XRD patterns of BFO-500 and BFO-600. The tartaric acid modified sol–gel method provides a simple low-temperature synthesis route for preparing pure phase $BiFeO_3$ [9]. The XRD pattern of the BFO-500 (Fig. 1(a)) shows that the $BiFeO_3$ powders have R3c structure without any impurity phase. However, there are always impurities in the final products before leaching in the diluted HNO_3 solution with cotton templates. The sintering temperature of 600 °C was selected as there was only impurity of $Bi_{25}FeO_{39}$ in the products and can be easily removed in the diluted HNO_3 solution. As can be seen in Fig. 1(b), the BFO-600 exhibits pure R3c structure without any impurity. The lattice parameters calculated from the XRD patterns are $a = 5.572$ Å and $c = 13.846$ Å for BFO-500, and $a = 5.582$ Å and $c = 13.873$ Å for BFO-600, indicating the lattice expansion of $BiFeO_3$ prepared using cotton templates. The grain size estimated by the Scherrer equation is about 30 nm for BFO-500, and 50 nm for BFO-600.

Fig. 2 shows the morphology of $BiFeO_3$ prepared with cotton templates by SEM. The sample exhibits the porous structure clearly. This is due to the porous structure of cotton fibers. The advantage of the cotton template is that it can be totally removed

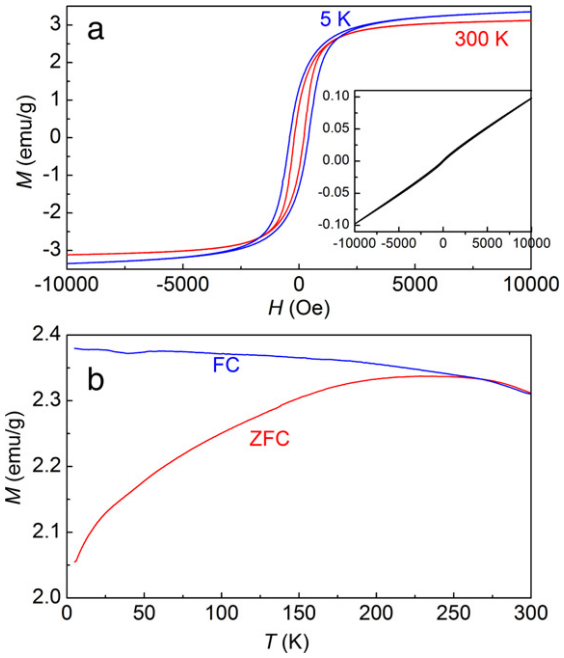

Fig. 3. (a) M–H curves of BFO-600 at 5 K and 300 K, inset shows the M–H curve of BFO-500 at 300 K. (b) ZFC and FC M–T curves of BFO-600.

during the sintering process, thus no further process needed to remove the template. The solution filled in the pores of the cotton fibers, and the growth of grains was confined. The porous structure can be seen more clearly in the enlarged view as shown in the top inset. However, the sample is fragile. After leaching in diluted HNO_3 solution, the porous $BiFeO_3$ was broken to much smaller pieces, but the porous structure was kept (bottom inset).

Fig. 3 shows the magnetic properties of BFO-600. As can be seen in Fig. 3(a), BFO-600 exhibits clear hysteresis loops at 5 K and 300 K, and the saturate magnetization is about 3 emu/g at 300 K. For comparison, the M–H curve at 300 K of BFO-500 is shown in the inset of Fig. 3(a), which exhibits the typical antiferromagnetic behavior with weak ferromagnetism as that of bulk $BiFeO_3$ [11], and the magnetization at 10 000 Oe is only about 0.1 emu/g. Fig. 3(b) shows the field cooled (FC) and zero field cooled (ZFC) M–T curves of BFO-600 measured at the field of 1000 Oe. The FC magnetization continues to increase with decreasing temperature, while ZFC magnetization shows a peak at around 235 K. Similar phenomenon has been observed in $BiFe_{0.95}Co_{0.05}O$ which has been attributed to the cluster spin glass transition [12]. A small anomaly at around 30 K is seen, which may be due to the spin reorientation [13].

Generally, the enhance magnetization in $BiFeO_3$ can be due to the suppression of the cycroidal spin structure with grain size smaller than the period of about 62 nm [5,6], thus larger magnetization can be achieved with smaller grain size. However, the grain size of BFO-600 (∼50 nm) is larger than that of BFO-500 (∼30 nm), and also the shape of M–H curve of BFO-600 with a much larger coercive field is different from those $BiFeO_3$ nanograins [5,6].

Fig. 4 shows the XPS profiles of Fe 2p in BFO-500 and BFO-600. The binding energy is calibrated by taking carbon C1s peak (284.8 eV) as Ref. [14]. The two Gaussians corresponding to Fe^{2+} and Fe^{3+} were fitted in the Fe $2p_{3/2}$ peak of BFO-500 (Fig. 4(a)) and BFO-600 (Fig. 4(b)). For BFO-500, the subpeak of Fe^{2+} locates at 709.67 eV and that of Fe^{3+} locates at 711.11 eV with Fe^{2+}/Fe^{3+} ratio of 38:62. For BFO-600, the subpeak of Fe^{2+} locates at 709.98 eV and that of Fe^{3+} locates at 711.49 eV with Fe^{2+}/Fe^{3+} ratio of 38:62. Thus there is the same amount of Fe^{2+} in BFO-500 and BFO-600.

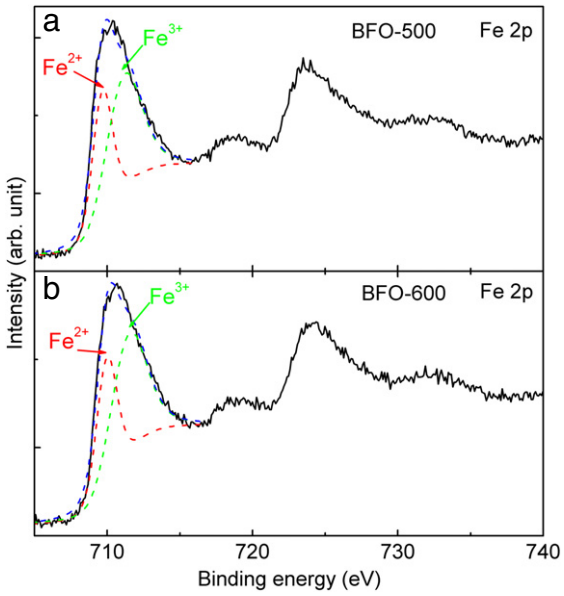

Fig. 4. The fitting XPS spectra of Fe 2p for (a) BFO-500 and (b) BFO-600.

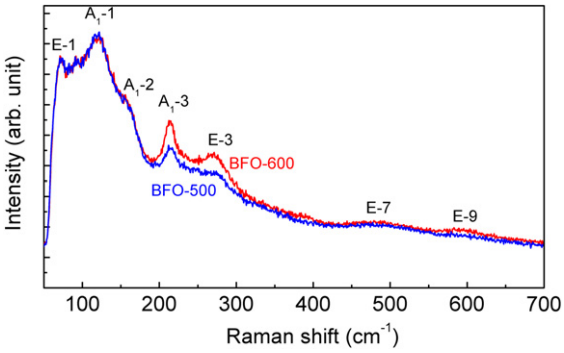

Fig. 5. Room temperature Raman spectra of BFO-500 and BFO-600.

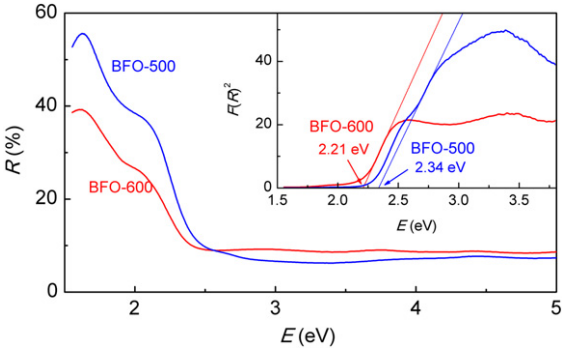

Fig. 6. Room temperature diffuse reflectance spectra of BFO-500 and BFO-600. The inset shows the plot of $F(R)^2$ versus E, and the thinner lines are the linear fitting to get the energy band gap.

Raman spectra were taken for BFO-500 and BFO-600 at room temperature, as shown in Fig. 5. All the Raman modes of both samples can be indexed to the modes of $BiFeO_3$ molecule with R3c structure [15]. BFO-500 and BFO-600 show almost identical curves, except for that the intensity of $A_1 - 3$ and E-3 modes for BFO-600 is significantly stronger than those of BFO-500. As indicated by Simões, the peaks of Raman shift higher than 200 cm^{-1} result from the FeO_6 octahedral [16]. The stronger intensity of the $A_1 - 3$ and E-3 modes for BFO-600 can be attributed to the oxygen octahedral tilts induced structural distortion.

Fig. 6 shows the UV–visible optical diffuse reflectance spectra of BFO-500 and BFO-600. It is clearly seen that the reflectance significantly decreased near the excitonic absorption edge for both samples, which are related to the optical band gap. For the purpose of analysis, the diffuse reflectance, R, of the sample can be related to the Kubelka–Munk function $F(R) = (1 - R)^2/2R$. The energy band gap can be obtained by plotting the $F(R)^2$ versus energy and extrapolating the linear part of the curve to $F(R)^2 = 0$ [17], as shown in the inset of Fig. 6. The band gap of BFO-500 is 2.34 eV, which is smaller than the reported value of about 2.67 eV for bulk $BiFeO_3$ [18], which might be due to the size effect, as smaller band gap observed in $BiFeO_3$ nanoparticles [19,20]. The band gap of BFO-600 is 2.21 eV, which is smaller than that of BFO-500. The decrease of band gap for BFO-600 might be explained by the suppressed tilt angle of the oxygen octahedra, which increase the Fe^{2+}–O–Fe^{3+} angle and forced higher symmetry is expected to increase the band width of occupied and unoccupied bands, reducing the band gap [21]. In $BiFeO_3$, the existence of Fe^{2+} has been generally considered as the source of the enhancement of ferromagnetism via the double exchange Fe^{2+}–O–Fe^{3+} interaction [22]. However, the ratio of Fe^{2+}/Fe^{3+} in BFO-500 and BFO-600 are the same, thus the enhancement of ferromagnetism should be attributed to the increased angle of Fe^{2+}–O–Fe^{3+}, which enhances the double exchange interaction [23].

4. Conclusions

In summary, porous $BiFeO_3$ has been prepared using cotton templates. Strongly enhanced ferromagnetism with saturate magnetization of 3 emu/g at 300 K has been observed. An energy band gap of 2.21 eV was determined from the UV–visible diffuse reflectance spectrum. The Raman and X-ray photoelectron spectroscopy measurements indicate the existence of Fe^{2+} and the suppression of the oxygen octahedral tilts. The enhanced ferromagnetism has been attributed to the enhanced double exchange interaction with increased angle of Fe^{2+}–O–Fe^{3+}.

Acknowledgements

We thank X. Lang for the Raman measurements. This work is supported by the National Natural Science Foundation of China (50802041, 50872050), National Key Projects for Basic Researches of China (2009CB929503, 2010CB923404), by NCET-09-0296 and Southeast University. M.X. Xu acknowledges the support from the Research Fund for the Doctoral Program of Higher Education of China (Grant No. 20070286037).

References

[1] Smolenskii G.A., I. Chupis, Sov. Phys. Usp. 25 (1982) 475.
[2] G. Catalan, J.F. Scott, Adv. Mater. 21 (2009) 2463.
[3] D. Lebeugle, D. Colson, A. Forget, M. Viret, A.M. Bataille, A. Gukasov, Phys. Rev. Lett. 100 (2008) 227602.
[4] H. Béa, M. Bibes, S. Petit, J. Kreisel, A. Barthélémy, Phil. Mag. Lett. 87 (2007) 165.
[5] R. Mazumder, P. Sujatha Devi, D. Bhattacharya, P. Choudhury, A. Sen, M. Raja, Appl. Phys. Lett. 91 (2007) 062510.
[6] T. Park, G.C. Papaefthymiou, A.J. Viescas, A.R. Moodenbough, S.S. Wong, Nano Lett. 7 (2007) 766.
[7] V.A. Khomchenko, D.A. Kiselev, M. Kopcewicz, M. Maglione, V.V. Shvartsman, P. Borisov, W. Kleemann, A.M.L. Lopes, Y.G. Pogorelov, J.P. Araujo, R.M. Rubinger, N.A. Sobolev, J.M. Vieira, A.L. Kholkin, J. Magn. Magn. Mater. 321 (2009) 1692.
[8] V.B. Naik, R. Mahendiran, Solid State Commun. 149 (2009) 754.
[9] S. Ghosh, S. Dasgupta, A. Sen, H.S. Maiti, J. Am. Ceram. Soc. 88 (2005) 1349.
[10] D. Lebeugle, D. Colson, A. Forget, M. Viret, P. Bonville, J.F. Marucco, S. Fusil, Phys. Rev. B 76 (2007) 024116.
[11] F. Wen, N. Wang, F. Zhang, Solid State Commun. 150 (2010) 1888.
[12] Q. Xu, S. Zhou, D. Wu, M. Uhlarz, Y.K. Tang, K. Potzger, M.X. Xu, H. Schmidt, J. Appl. Phys. 107 (2010) 093920.
[13] B. Ramachandran, M.S. Ramachandra Rao, Appl. Phys. Lett. 95 (2009) 142505.
[14] L. Wei, Z. Li, W.F. Zhang, Appl. Surf. Sci. 255 (2009) 4992.

[15] Y. Yang, J.Y. Sun, K. Zhu, Y.L. Liu, L. Wan, J. Appl. Phys. 103 (2008) 093532.
[16] A.Z. Simões, E.C. Aguiar, A.H.M. Gonzalez, J. Andrés, E. Longo, J.A. Varela, J. Appl. Phys. 104 (2008) 104115.
[17] M. Naeem, S. Qaseen, I.H. Gul, A. Maqsood, J. Appl. Phys. 107 (2010) 124303.
[18] R. Chen, N.J. Podraza, X.S. Xu, A. Melville, E. Vlahos, V. Gopalan, R. Ramesh, D.G. Schlom, J.L. Musfeldt, Appl. Phys. Lett. 96 (2010) 131907.
[19] F. Gao, X. Chen, K. Yin, S. Dong, Z. Ren, F. Yuan, T. Yu, Z. Zou, J. Liu, Adv. Mater. 19 (2007) 2889.
[20] S. Li, Y. Lin, B. Zhang, Y. Wang, C. Nan, J. Phys. Chem. C 114 (2010) 2903.
[21] A.Y. Borisevich, H.J. Chang, M. Huijben, M.P. Oxley, S. Okamoto, M.K. Niranjan, J.D. Burton, E.Y. Tsymbal, Y.H. Chu, P. Yu, R. Ramesh, S.V. Kalinin, S.J. Pennycook, Phys. Rev. Lett. 105 (2010) 087204.
[22] F.P. Gheroghiu, A. Ianculescu, P. Postolache, N. Lupu, M. Dobromir, D. Luca, L. Mitoseriu, J. Alloys Compd. 506 (2010) 862.
[23] N. Badelmoula, J. Dhahri, K. Guidara, E. Dhahri, J.C. Joubert, Phase Transit. 70 (1999) 197.